A simple theory of angle-resolved photoemission spectroscopy cross sections with applications to $YBa_2Cu_3O_7$ and Sr_2RuO_4

1998 J. Phys.: Condens. Matter 10 5197

(http://iopscience.iop.org/0953-8984/10/23/020)

J. Phys.: Condens. Matter **10** (1998) 5197–5216. Printed in the UK PII: S0953-8984(98)88192-7

A simple theory of angle-resolved photoemission spectroscopy cross sections with applications to $YBa_2Cu_3O_7$ and Sr_2RuO_4

E Seibel and H Winter

Forschungszentrum Karlsruhe, Institut für Nukleare Festkörperphysik, Postfach 3640, D-76021, Germany

Received 6 October 1997, in final form 26 January 1998

Abstract. We try to interpret angle-resolved photoemission spectroscopy (ARPES) cross sections directly in band-structure terms by approximating the one-particle propagator needed to evaluate the lowest-order Keldysh diagram using the bulk Green function. As applications to $YBa_2Cu_3O_7$ and Sr_2RuO_4 demonstrate, this is a sensible approach, since it reproduces important features of experimental curves. Matrix element effects strongly enhancing the contributions of individual bands at certain energies and depressing them at others are well described. Self-energy corrections included in an average way improve the agreement and allow for a rough estimate of the magnitude of the band broadening. In the case of $YBa_2Cu_3O_7$ our investigations demonstrate the significance of correlations, since adding self-interaction corrections to the local density approximation leads to considerable improvement of the calculated ARPES cross sections.

1. Introduction

Angle-resolved photoemission spectroscopy (ARPES) has developed into a powerful tool for investigating the electronic structures of a variety of materials with complicated physical properties (see, e.g., Veal and Gu 1994, Shen and Dessau 1995), since in principle it is able to detect individual states and trace band dispersions. A great number of these experiments were carried out to study bulk properties. Since the electrons contributing to the photocurrent are predominantly emitted from a few near-surface layers of atoms, this method is, however, highly surface sensitive. Due to great achievements in sample preparation, crystals with clean and well defined surfaces are now available for the measurements.

On the theoretical side, formalisms and corresponding codes have been developed and applied taking account of this more complicated situation in comparison to that of experiments observing electrons escaping from deeper regions. These methods describe the photoemission process in second-order perturbation theory with respect to the vector potential of the photon field and are based on the diagram technique of Keldysh (1965), worked out by Feibelman and Eastman (1974), or equivalent formulations. The methods most frequently used rest on the work of Pendry (1976), treating the lowest-order diagram and gaining the electron propagators occurring by applying one-particle scattering theory to the half-space occupied by the sample. Later on, this formulation was adapted and applied to the description of more complex systems (see, e.g., Lindroos and Bansil 1991). As input parameters, the site-dependent potentials or single-site scattering matrices are required. At

0953-8984/98/235197+20$19.50

the highest level of sophistication a full, self-consistent surface calculation should provide these quantities, whilst in most cases they are actually approximated by their bulk values even for near-surface sites.

This kind of consideration may give the impression that extensive calculations are indispensable when trying to establish any explicit connection between features of measured cross sections and bulk electronic structures represented, e.g., by bands and electronic states. On the other hand, there exist many experimental papers in which the authors try with surprising success to explain the main features of their results directly in terms of these quantities without resorting to any detailed calculation. This observation motivated us to test the capability of a photoemission theory that approximates—at variance with the aforementioned methods—the one-particle propagator of the occupied energy range in the lowest-order Keldysh diagram by the bulk band-structure Green function.

In section 2 we describe this formalism and we apply it to $YBa_2Cu_3O_4$, a compound of considerable current interest, in section 3. Using our calculated LDA (local density approximation) and LDA–SIC (local density approximation with self-interaction corrections) band structures we evaluate cross sections for extended and near-Fermi-energy regions, respectively, and compare them to experiment. Similar investigations on the basis of our LDA band structure are undertaken for Sr_2RuO_4 in section 4, and we conclude with a summary in section 5.

2. Formalism

To calculate ARPES cross sections to second order in the amplitude of the applied photon field we use Keldysh's diagram technique (Keldysh 1965). The contribution of the lowest-order diagram to the photoelectron current in the observation direction $\boldsymbol{e}_r$ is proportional to the following expression (Feibelman and Eastman 1974):

$$\boldsymbol{j}(\boldsymbol{r}) \propto \lim_{\boldsymbol{r}\to\boldsymbol{r}'\to\infty} (\boldsymbol{e}_r \cdot \boldsymbol{\nabla}_r - \boldsymbol{e}'_r \cdot \boldsymbol{\nabla}'_r) \int \mathrm{d}\boldsymbol{r}_1\ \mathrm{d}\boldsymbol{r}_2\ g^{ret}(\boldsymbol{r}, \boldsymbol{r}_1; E) \times g^{adv}(\boldsymbol{r}_2, \boldsymbol{r}'; E)(\boldsymbol{A}_{sc}(\boldsymbol{r}_1) \cdot \boldsymbol{\nabla}_{r_1})(\boldsymbol{A}_{sc}(\boldsymbol{r}_2) \cdot \boldsymbol{\nabla}_{r_2}) g_{-+}(\boldsymbol{r}_1, \boldsymbol{r}_2; E - \omega). \quad (1)$$

Here, E is the energy of the photoelectrons, ω is the frequency of the photon field and $\boldsymbol{A}_{sc} = a\boldsymbol{e}_p \exp(\mathrm{i}\boldsymbol{k}_\gamma \cdot \boldsymbol{r})$ its screened vector potential. The integrals extend over the volume of the solid, assumed to occupy the half-space $z < 0$.

Following Feibelman and Eastman, we express the Green functions g^{ret} and g^{adv} through the LEED state $\Phi_>$, obtaining

$$r^2 \boldsymbol{j}(\boldsymbol{r}) \propto \boldsymbol{e}_r \sqrt{E} \int \mathrm{d}\boldsymbol{r}_1\ \mathrm{d}\boldsymbol{r}_2\ \Phi_>(\boldsymbol{r}_1, \boldsymbol{k})(\boldsymbol{A}_{sc} \cdot \boldsymbol{\nabla}_{r_1}) \times \Phi^*_>(\boldsymbol{r}_2, \boldsymbol{k})(\boldsymbol{A}_{sc} \cdot \boldsymbol{\nabla}_{r_2}) g_{-+}(\boldsymbol{r}_1, \boldsymbol{r}_2; E - \omega) \quad (2)$$

with

$$\boldsymbol{k} = \sqrt{E}\boldsymbol{e}_r.$$

$\Phi_>$ may be determined by solving the following equation:

$$\Phi_>(\boldsymbol{r}, \boldsymbol{k}) = \exp(\mathrm{i}\boldsymbol{k} \cdot \boldsymbol{r}) + \int \mathrm{d}\boldsymbol{r}'\ g^{ret}(\boldsymbol{r}, \boldsymbol{r}'; E) V(\boldsymbol{r}') \exp(\mathrm{i}\boldsymbol{k} \cdot \boldsymbol{r}'). \quad (3)$$

Equation (3) is valid for electrons moving in an effective one-particle potential, provided, e.g., by density functional (DF) theory. Self-energy corrections, not included in equation (3), however, turn out to be important. Their most significant effect is a rapid decay of $\Phi_>$

towards the interior of the solid. This leads us to replace the plane waves $\Phi_{>}^{(0)}(\boldsymbol{r}, \boldsymbol{k}) = \exp(\mathrm{i}\boldsymbol{k}\cdot\boldsymbol{r})$ with damped waves inside the solid:

$$\Phi_{>}^{(0,d)}(\boldsymbol{r}, \boldsymbol{k}) = \exp[\mathrm{i}\boldsymbol{k}\cdot\boldsymbol{r} + \Gamma(E)\boldsymbol{r}\cdot\boldsymbol{n}/(2\boldsymbol{n}\cdot\boldsymbol{e}_r)]. \tag{4}$$

Here, $\boldsymbol{n}$ is a unit vector perpendicular to the surface of the solid and pointing to the vacuum side. Since Γ is some spatial average of the self-energy Σ, the potential in equation (3) should be replaced with the complex quantity $V + \mathrm{i}\Gamma$. Extracting actual numbers for Γ from the average curves of Ley and Cardona (1979), we conclude that the escape depth of the photoelectrons in the energy range covered by the experiments discussed in the present paper is of the order of only a few atomic layers.

The interesting information concerning the electronic properties of the solid is contained in the Green function g_{-+}, describing the occupied part of the energy spectrum, and our aim is to investigate whether it makes sense to interpret ARPES experiments in terms of its bulk expression, written in the following form:

$$g_{-+}(\boldsymbol{r}_1, \boldsymbol{r}_2; \varepsilon) = \sum_{\lambda} \int (\mathrm{d}\boldsymbol{q}/\Omega_{BZ})\ \Psi_{\boldsymbol{q}\lambda}(\boldsymbol{r}_1)\Psi^{*}_{\boldsymbol{q}\lambda}(\boldsymbol{r}_2) g_{(-+)\boldsymbol{q}\lambda}(\varepsilon) \tag{5}$$

with

$$g_{(-+)\boldsymbol{q}\lambda}(\varepsilon) = \frac{(\operatorname{Im}\Sigma_{\boldsymbol{q}\lambda}(\varepsilon))\Theta(-\varepsilon - \Phi)}{[\varepsilon - \varepsilon_{\boldsymbol{q}\lambda} - \operatorname{Re}\Sigma_{\boldsymbol{q},\lambda}(\varepsilon)]^2 + [\operatorname{Im}\Sigma_{\boldsymbol{q},\lambda}(\varepsilon)]^2}.$$

Here, Φ is the work function of the material, $\boldsymbol{q}, \lambda$ are the quantum numbers of the one-particle states $\Psi_{\boldsymbol{q}\lambda}$ with energy $\varepsilon_{\boldsymbol{q}\lambda}$, and $\Sigma_{\boldsymbol{q}\lambda}$ are the diagonal matrix elements of the self-energy connecting these states, the off-diagonal ones being safely negligible for the substances discussed in this paper.

Finally, we subdivide the solid into layers parallel to its surface, labelling the atoms in the two-dimensional unit cell of layer m at position $\boldsymbol{r}_m^{(0)}$ with the indices κ, m. The coordinates of a site (κ, m, j) are then given by the following relation:

$$\boldsymbol{r}_{m\kappa,j} = \boldsymbol{r}_m^{(0)} + \boldsymbol{R}_j + \boldsymbol{\tau}_{\kappa,m} \qquad \text{with } \boldsymbol{R}_j = \sum_{j=1,2} n_j \boldsymbol{a}_j. \tag{6}$$

Here, the $\boldsymbol{a}_j$ are basis vectors of the corresponding two-dimensional Bravais lattice, and $\boldsymbol{\tau}_{\kappa,m}$ is the local atomic coordinate. For simplicity we assume in the following that the vectors $\boldsymbol{a}_j$ coincide with two of the lattice vectors of the extended solid.

Inserting equations (5) and (6) into equation (2) and performing the two-dimensional lattice sum we obtain

$$r^2\boldsymbol{j}(\boldsymbol{r}) \propto \boldsymbol{e}_r\sqrt{E}\sum_{\lambda}\int (\mathrm{d}\boldsymbol{q}/\Omega_{BZ})\ \delta(\boldsymbol{q}_{\parallel} - \boldsymbol{k}_{\parallel} + \boldsymbol{G})|M_{\lambda}(\boldsymbol{q}, \boldsymbol{k})|^2 g_{(-+)\boldsymbol{q}\lambda}(E - \omega). \tag{7}$$

Here, $\boldsymbol{q}_{\parallel}$ and $\boldsymbol{k}_{\parallel}$ are the components of $\boldsymbol{q}$ and $\boldsymbol{k}$ parallel to the surface, and $\boldsymbol{G}$ is the reciprocal-lattice vector reducing $\boldsymbol{k}_{\parallel}$ to the first Brillouin zone (BZ). Momentum conservation is thus imposed on only two components of $\boldsymbol{q}$, whereas the finite lifetime of the LEED state implies performing a weighted integral over the third one. In practice, the broadening of the third component amounts to 5 to 20% of the linear extent of the BZ. The matrix element, $M_{\lambda}(\boldsymbol{q}, \boldsymbol{k})$, is defined through the relation

$$M_{\lambda}(\boldsymbol{q}, \boldsymbol{k}) = \sum_{m,\kappa}\int \mathrm{d}\boldsymbol{\rho}\ \Phi_{>}(\boldsymbol{\rho} + \boldsymbol{r}_m^{(0)} + \boldsymbol{\tau}_{\kappa,m}, \boldsymbol{k}) \times (\boldsymbol{A}_{sc}\cdot\boldsymbol{\nabla}_{\boldsymbol{\rho}})\Psi_{\boldsymbol{q}\lambda}(\boldsymbol{\rho} + \boldsymbol{\tau}_{\kappa,m})\exp(\mathrm{i}\boldsymbol{q}\cdot(\boldsymbol{r}_m^{(0)} + \boldsymbol{\tau}_{\kappa,m})). \tag{8}$$

The integral in equation (8) extends over the Wigner–Seitz (WS) cells of the atoms κ, m, and the states $\Psi_{\boldsymbol{q},\lambda}$ are assumed to be given in the Bloch representation:

$$\psi_{\boldsymbol{q}\lambda}(\boldsymbol{\rho}+\boldsymbol{\tau}_{\kappa,m}) = \sum_{ln} c^{(\kappa,m)}_{ln,\boldsymbol{q}\lambda} R^{(\kappa,m)}_{l}(\rho, \varepsilon_{\boldsymbol{q}\lambda}) Y_{ln}(\boldsymbol{\rho}). \tag{9}$$

Due to the decay of $\Phi_{>}$, expressed by equations (3) and (4), the sum over m contributes significantly for only a few surface layers. The contributions of the individual atoms to M_λ are modulated by a phase factor, turning out to be of considerable significance for the interpretation of ARPES cross sections. In the applications of the present paper we approximate $\Phi_{>}$ by the damped plane wave (equation (4)), since a perturbative treatment of the second term hardly changed the results. We also take into account the finite experimental resolutions in energy and escape angle by convoluting expression (7) with the resolution functions applying to the experiment under consideration. Higher-order processes, not contained in this lowest-order dressed Keldysh diagram, give rise to the essentially unstructured background found in experimental cross sections, which grow on increasing the binding energies. When comparing our theoretical results to experiment, we subtract them off.

3. Calculations for $YBa_2Cu_3O_7$

3.1. The LDA band structure

There have been a host of LDA band-structure studies of this compound. (See, e.g., Pickett (1989) and citations therein.) In spite of the fact that LSDA fails for $YBa_2Cu_3O_6$, yielding a metallic instead of the observed antiferromagnetic insulating ground state, LDA seems to work in the case of $YBa_2Cu_3O_7$, at least as far as Fermi surface (FS) properties are concerned.

The results of our LMTO–ASA calculations are in general agreement with those cited above, though the Fermi surface we derive differs in some more subtle details from the more advanced calculations of Pickett *et al* (1990). Two essentially planar Cu (Cu2)–planar O (O2, O3)-dominated bands and one mainly chain Cu(Cu1)-dominated band cross the Fermi level, giving rise to a relatively low DOS value of 44.4 states Ryd^{-1}/unit cell. As figure 1—displaying the total as well as site-dependent partial DOS—shows, the Cu and the O atoms yield the main contributions to the spiky, 5.5 eV broad high-DOS region below ε_F, while the Y and Ba partial DOS start to dominate beyond the 0.7 eV broad gap above ε_F. The characters of the state coefficients $c_{\boldsymbol{q}\lambda}$ are considerably hybridized and vary rapidly when $\boldsymbol{q}$ moves through the BZ, leading to a sensitive dependence of the matrix elements $M_{\boldsymbol{q}\lambda}$ on the $\boldsymbol{q}$-point probed by the ARPES measurement. In connection with these experiments, a bandwise decomposition of the DOS, as indicated by the broken lines in figure 1(a), may also be of interest.

3.2. The LDA–SIC band structure

In addition to this LDA work we performed band-structure calculations including self-interaction corrections (SIC). The formalism underlying these investigations is described by Temmerman *et al* (1993) and has been successfully applied to a variety of systems (see, e.g., Szotek *et al* 1993, 1994) and is equivalent to that developed by Svane and Gunnarsson (Svane and Gunnarsson 1990, Svane 1992). In this approach one distinguishes between states essentially localized at individual sites and described by Wannier functions on the one hand and extended Bloch states on the other. SI corrections are important for the former

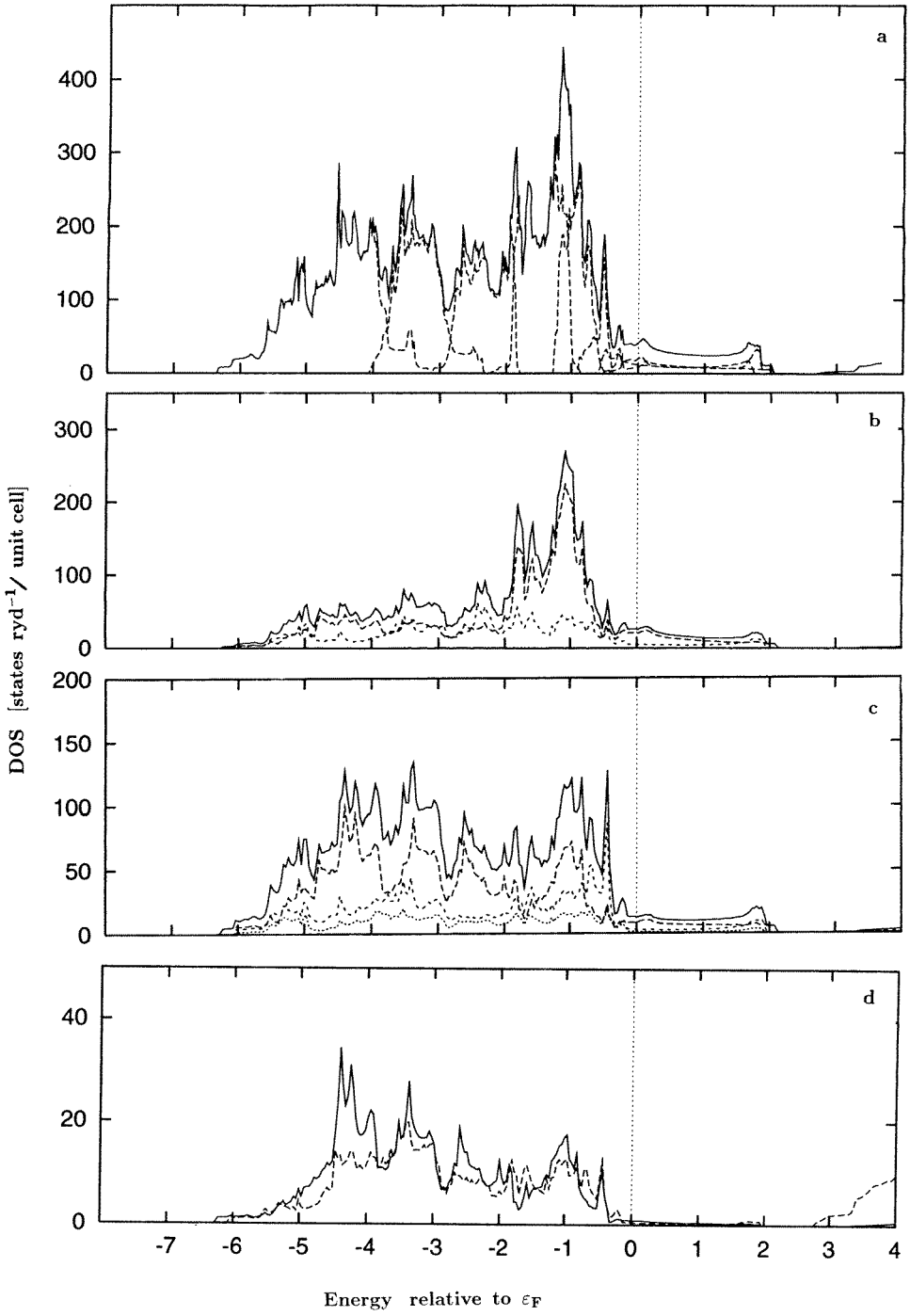

Figure 1. The LDA band structure of $YBa_2Cu_3O_7$: densities of states. (a) Total DOS; broken lines: contributions of the following groups of bands: 1–10, 11–16, 17–21, 22–28, 29–32, 33, 34, 35, 36. (b) Partial DOS of Cu: solid line: total; – – –: planar Cu; - - - -: chain Cu. (c) Partial DOS of O: solid line: total; – – –: planar O; ·····: chain O; - - - -: apex O. (d) Partial DOS of Y (solid line) and Ba.

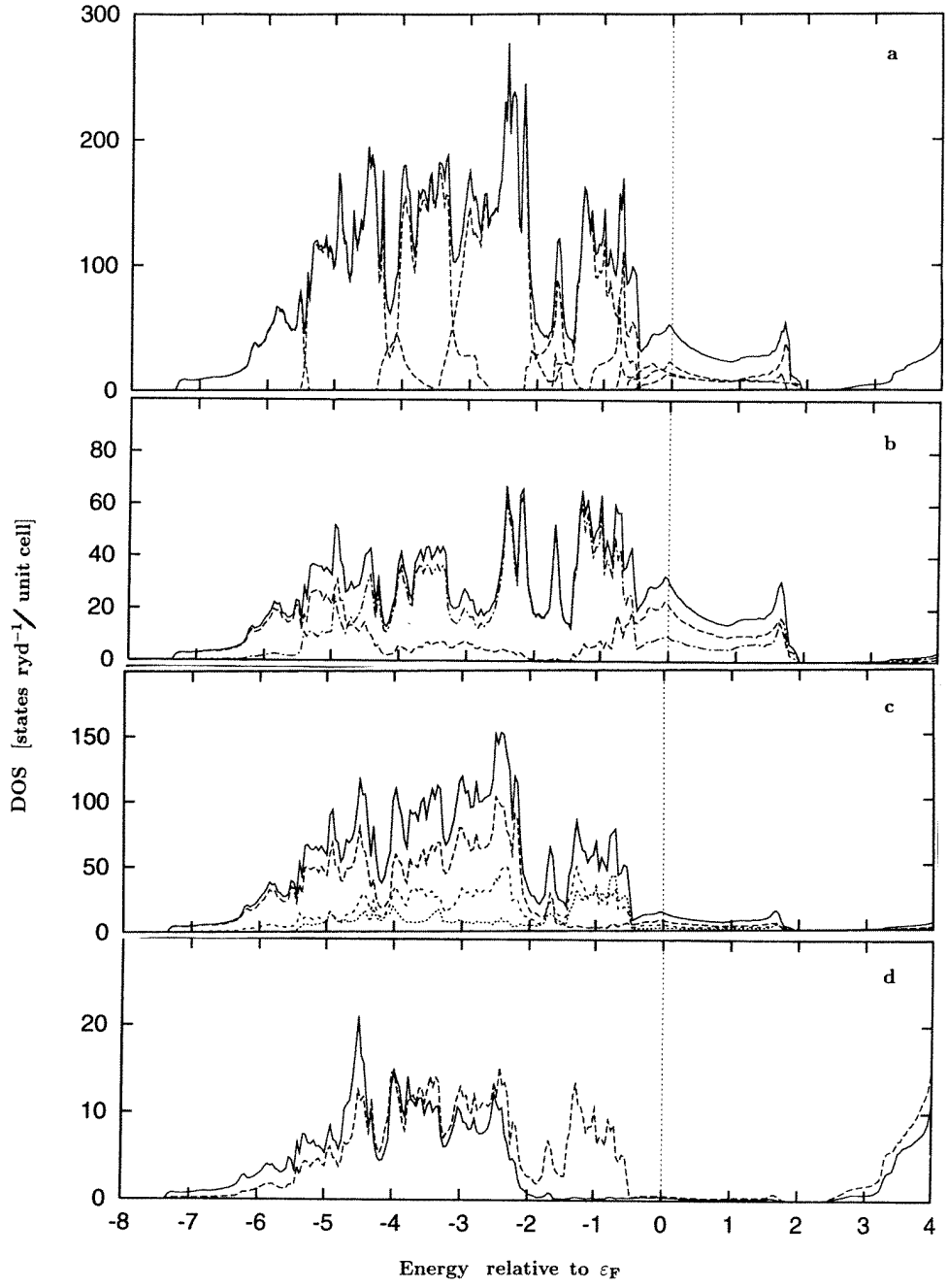

Figure 2. The LDA–SIC band structure of $YBa_2Cu_3O_7$: densities of states. (a) Total DOS; broken lines: contributions of the following groups of bands: 9–10, 11–16, 17–21, 22–28, 29, 30–32, 33, 34, 35, 36. (b) Partial DOS of Cu: solid line: total; – – –: planar Cu; — · —: chain Cu. (c) Partial DOS of O: solid line: total; – – –: planar O; ·····: chain O; - - - -: apex O. (d) Partial DOS of Y (solid line) and Ba.

category of states only. In practical applications one performs a series of self-consistent calculations using different sets of localized states and considers the configuration yielding the lowest ground-state energy as the physically relevant one.

In the case of $YBa_2Cu_3O_7$ it turned out energetically favourable to merely self-interaction correct a certain number, n_d, of planar Cu d states. The energy minimum occurred for $n_d = 8$ and was found to lie 0.53 Ryd/unit cell below the LDA result. The numbers, on the other hand, obtained from calculations choosing $n_d = 2$, 4, 6 and 10, turned out to fall at least 1 Ryd/unit cell above the minimum. In the following we employ the data corresponding to $n_d = 8$.

In the occupied energy region we find eight extremely tight bands of predominantly planar Cu d character located at 13.5 to 12.8 eV below ε_F and separated from the rest of the states by a gap of 4.5 eV. In figure 2 we show the LMTO–SIC DOS for the same energy range as for the LDA results. Bands 9 to 36 spread over roughly the same energy range as bands 1 to 36 in the LDA case. The FS remains to be built up by bands 34 to 36. Whereas the topology of the FS sheet of band 34 hardly changes in comparison to the LDA, the differences for bands 35 and 36 are more substantial, since they are flattened by the SI corrections. The DOS at ε_F is again relatively low ($n(\varepsilon_F) = 46.6$ states Ryd^{-1}/unit cell). More important differences between the LDA and the LDA–SIC results become apparent with increasing distance from ε_F as may be seen by comparing figures 1 and 2, exhibiting marked differences in their peak structures. Due to the splitting of the Cu d bands, the SIC partial Cu DOS and as a consequence the total SIC DOS are substantially reduced below the LDA DOS values. Since SIC diminishes the planar Cu–planar O hybridization, the partial oxygen DOS are also affected. For comparison to the LDA results, the contributions of individual groups of bands to the SIC DOS are also displayed in figure 2(a).

3.3. The evaluation of ARPES cross sections

Our goal is to investigate whether calculations based on equation (7) are in principle useful for interpreting measured cross sections. If this is the case, we are also in a position to see whether our application of the LMTO–SIC technique to YBa_2Cu3O_7 leads to an improvement over the LDA results. Instead of trying to give a full account of the great number of experiments performed for this compound we therefore concentrate on a few examples.

To make contact with a measurement of Sakisaka *et al* (1989), we assume the surface to be perpendicular to the c-axis and—since the crystals used in this experiment are twinned—we average over the orientations of the a- and b-axes. The photon frequencies of this experiment treated in our calculations are $\omega = 25$, 30, 42, and 50 eV, $\boldsymbol{e}_r$ is parallel to the c-axis, the angle between $\boldsymbol{k}_\gamma$ and the c-axis amounts to 60°, and $\boldsymbol{e}_p$ is in the a, b-plane. Thus the states at wave vectors $\boldsymbol{q} = (0, 0, q_z)$ in the BZ are probed by this experiment. To perform the calculations, we need some information on the nature of the upper surface layers. Following Schroeder *et al* (1993) we assume that the crystal has been cleaved at the energetically most favourable position, namely between the Ba atoms and the Cu–O plane. Unfortunately, the two crystal faces produced in this way are not identical: the topmost layer of one of them (sample a) consists of apex oxygen and Ba sites, whereas the surface of the other one (sample b) is a Cu–O plane. Our calculations, performed for both cases, show that the results differ significantly and that it is possible to determine which sample has been used in the measurement.

In figure 3 we display results obtained without applying any self-energy corrections. Whereas figures 3(a) and 3(b), referring to sample a and sample b, respectively, are

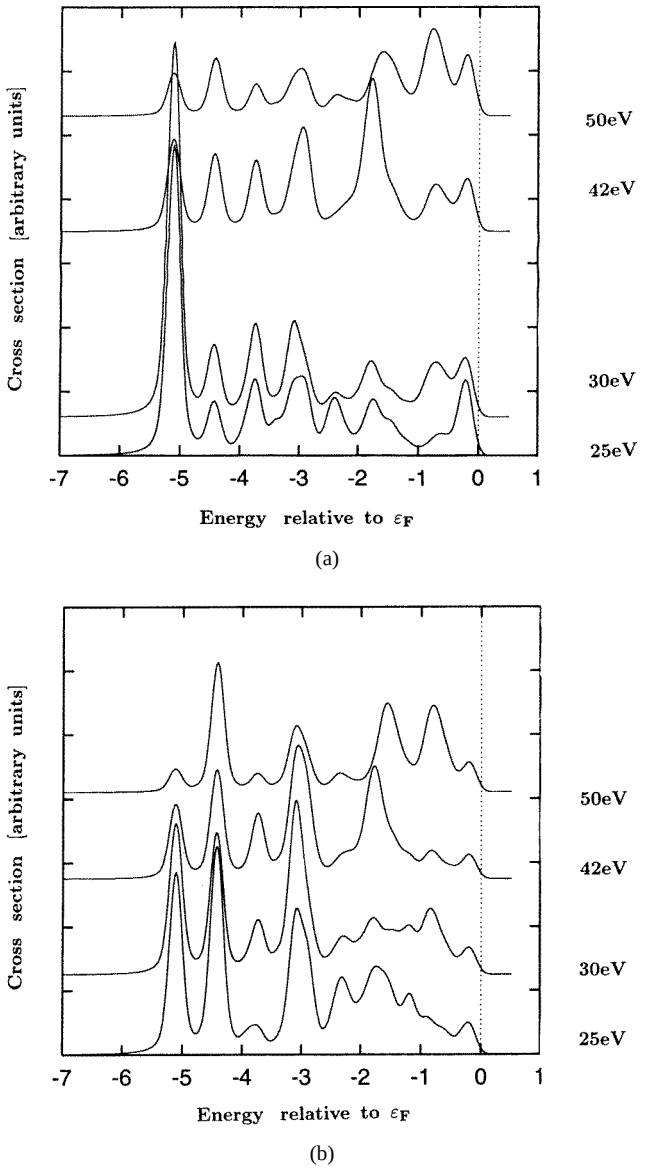

Figure 3. The unbroadened ARPES cross section of $YBa_2Cu_3O_4$ for photon energies between 25 eV and 50 eV, calculated using the LDA band structure. (a) The surface layer consists of Y and Ba atoms (sample a). (b) The surface layer is a Cu–O plane (sample b).

obtained using the LMTO band structure, figures 4(a) and 4(b) are based on the LMTO–SIC band structure. In spite of the fact that no band broadening enters the calculations at this step, the structures of the theoretical cross sections are more strongly washed out than the instrumental resolution (0.1 to 0.2 eV) can explain. As the DOS curves show, this is due to the high density of bands for the binding energies considered, preventing the experiment from detecting individual bands. Most striking is the marked dependence on the photon energy of the amplitudes of some of the peaks in these curves. Our analysis allows for

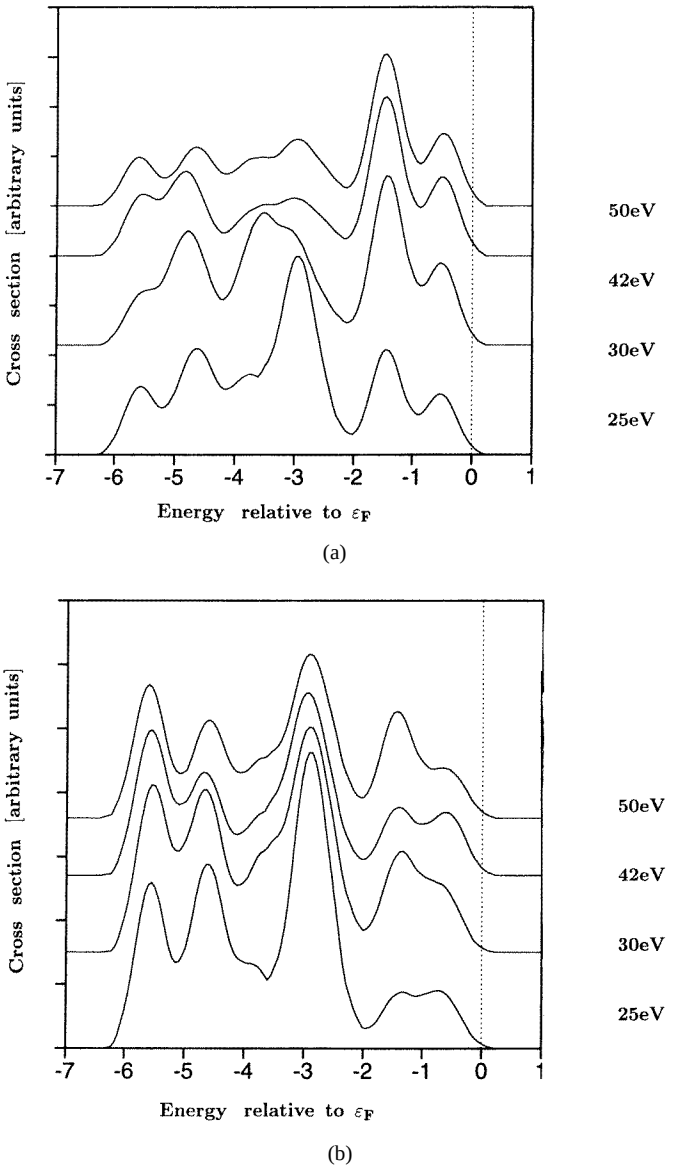

Figure 4. The unbroadened ARPES cross section of $YBa_2Cu_3O_4$ for photon energies between 25 eV and 50 eV, calculated using the LDA–SIC band structure. (a) The surface layer consists of Y and Ba atoms (sample a). (b) The surface layer is a Cu–O plane (sample b).

a quantitative explanation of this phenomenon: the matrix elements (equation (8)) are the sums of contributions from the individual atomic sites and depend on the vectors $\boldsymbol{k}$ and $\boldsymbol{q}$. For a given binding energy the magnitude of $\boldsymbol{k}$ varies with photon frequency ω. At certain binding energies the relative phases of these contributions vary strongly with ω giving rise to either constructive or destructive interference effects. As already mentioned above, the cross sections of sample a and sample b look quite different in the LDA and the SIC case. Furthermore, the LDA and the LDA–SIC results are fundamentally dissimilar.

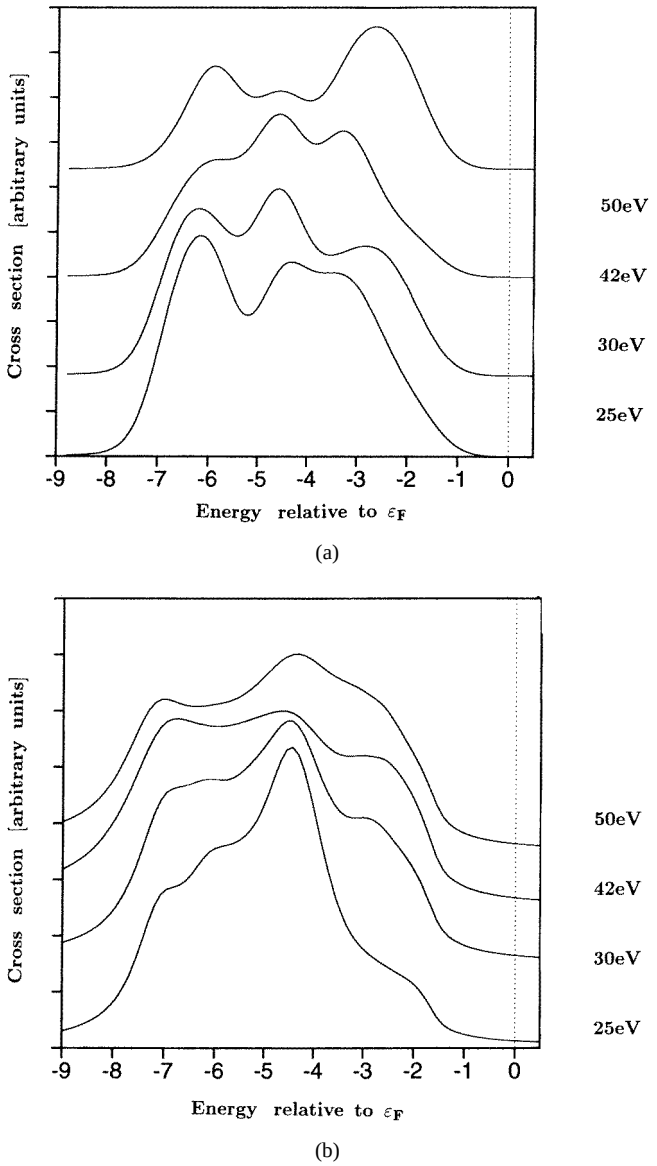

Figure 5. The ARPES cross sections of figures 3(b) and 4(b), including average band broadening. (a) LDA band-structure-based calculations. (b) LDA–SIC band-structure-based calculations.

Comparing these calculated cross sections with the results of Sakisaka *et al* (1989) (figure 1 in that paper), we find that only the cross sections for sample b, and based on the LMTO–SIC band structure, share the main features with the experimental curves. Especially gratifying is the fact that our theory explains the dramatic photon energy dependence of the amplitude of the intermediate peak near 3 eV observed in the experiment. The experimental cross sections, however, show considerably larger broadening than the theoretical ones. We try to account for this feature by including self-energy effects. For this purpose we approximate Im Σ in equation (5) by an average value Γ_Σ, except in the immediate vicinity

of ε_F, where it rapidly drops to zero. Choosing Γ_Σ to fit the experimental width of the intermediate peak of the $\omega = 42$ eV curve, we obtain the value $\mathrm{Im}\,\Sigma = 0.8$ eV, a number of reasonable order of magnitude. The self-energy-corrected results for sample b, obtained using this simple approximation for Σ and based on the LDA (figure 5(a)) and the LDA–SIC (figure 5(b)) band structures, are displayed in figure 5. While the curves corresponding to the LDA–SIC band structure are in reasonable agreement with experiment, the LDA-based ones differ substantially.

As a second example we investigate the electronic structure in the vicinity of the X, the Y and the Γ point, addressing an experiment of Tobin *et al* (1992). These authors used untwinned crystals and worked with resolutions of 32 meV in energy and 1° in angle. Referring to the coordinate system spanned by the crystallographic a-, b- and c-axes, the parameters of this experiment (figure 2 of their paper) are $\omega = 24$ eV, $\boldsymbol{k}_\gamma/k_\gamma = (-\sin\alpha, 0, \cos\alpha)$, $\boldsymbol{e}_p = (\cos\alpha, 0, \sin\alpha)$ with $\alpha = 40^\circ$, and $\boldsymbol{e}_r$ is given by (0, 0, 1) for the Γ-point curve, by (0.364, 0, 0.931) for the X-point curve and by (0, 0.358, 0.934) for the Y-point curve.

The measurement of Tobin *et al*, investigating the neighbourhood of the Γ point, could be expected to be comparable to the 25 eV curve of Sakisaka *et al*, since the photon energies of the two experiments are close. In spite of the fact that the differences in photon polarization complicates the comparison of these two experiments, and as Tobin *et al* show, the shape of the measured cross section at the S point of the BZ is considerably polarization dependent; a possible cause for this fundamental discrepancy at the Γ point might be that, unlike Sakisaka *et al*, Tobin *et al* used sample a. Our calculations, employing the LMTO–SIC band structure for the case of sample a, support this assumption. We again took account of band broadening, and $\Gamma_\Sigma = 0.7$ eV, a value consistent with and close to that used to fit the measurements of Sakisaka *et al*, turned out to be the optimum choice for reproducing the widths of the measured curves.

The results, shown in figure 6, reproduce the essential features of the measurements.

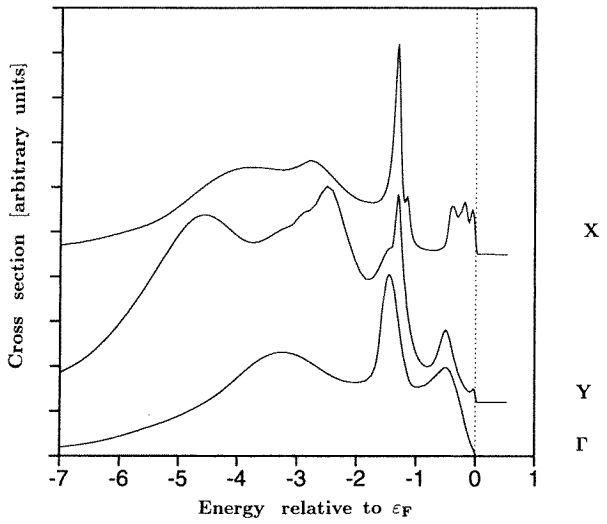

Figure 6. The ARPES cross sections of $YBa_2Cu_3O_7$ (sample a) in the neighbourhood of the X, the Y and the Γ point, evaluated using the LDA–SIC band structure, and including band broadening.

In no case are the pronounced peaks near 1.1 eV below ε_F indications of a single, almost dispersionless band, since they are caused by bands 29 and 30, by bands 30 and 31, and by bands 31 and 32 in the curves probing the vicinity of the Γ, the X and the Y point. Also the broad shoulders at higher binding energies are in correspondence with the observed structures. The humps appearing in the two lowest theoretical curves, at 0.5 eV below ε_F and caused by band 32, however, are at variance with the experiment. It is our aim to repeat the present calculations by using a band structure describing the near-Fermi-energy region more precisely and then to discuss this point in more detail.

In a series of experiments, Manzke *et al* (1991) also observed and investigated the nature of these sharp distinct peaks. They interpret them as the manifestation of surface states. To corroborate this hypothesis they demonstrated the high sensitivity of these peaks to surface damage and contamination (Manzke *et al* 1992, Harm *et al* 1992). We are not in the position to argue as regards the conclusiveness of their reasoning. We merely state that our theoretical investigations, omitting surface states, lead to similar structures. Maybe surface contamination destroys the property of $YBa_2Cu_3O_7$ of exhibiting bulk features in layers rather close to the surface.

Finally, we discuss an experiment of Liu *et al* (1992). In figure 5(a) of their paper they display the results of measurements investigating the neighbourhood of the FS in the Γ–S direction down to binding energies of 0.7 eV. They used twinned crystals and achieved resolutions of 55 meV and 2°, respectively. The appropriate parameters are: $\omega = 21.2$ eV, $\boldsymbol{k}_\parallel = (1, 1)0.514\sqrt{E}\sin\alpha$ (Å) with α varying from 0° to 12°. The values of $\boldsymbol{k}_\gamma/k_\gamma$ and $\boldsymbol{e}_p$ are the same as in the experiment of Tobin *et al*.

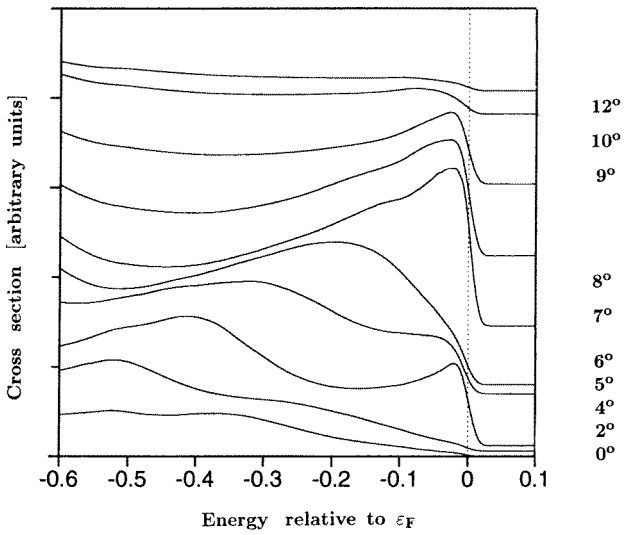

Figure 7. The ARPES cross sections of $YBa_2Cu_3O_7$ (sample b) in the near-FS region, evaluated using the LDA–SIC band structure, and including band broadening.

In the following we discuss theoretical curves obtained for sample b. They are again based on the LDA–SIC, leading to far better results than the LDA alone. The contributions to these cross sections come from bands 33 to 36. To interpret the experimental results in a satisfactory way we found it desirable to account for band broadening in more detail. To this end, we performed model calculations assuming the electrons—described by the LMTO–SIC band-structure Green function—to interact with low-frequency excitations via a contact

potential. In $YBa_2Cu_3O_7$, probably spin fluctuations, with especially large amplitudes near the BZ boundary in the (1, 1, 0) direction, contribute most efficiently to this mechanism. These investigations showed that—irrespective of the details of the excitation spectra used—Im $\Sigma(\varepsilon)_\lambda$, averaged over the energy surface ε of band λ, scales approximately with the partial DOS, $n_\lambda(\varepsilon)$, of this band, apart from in the energy region $\varepsilon - \varepsilon_F < \Delta\Omega$ (the spectral width of the excitations), where Im Σ_λ diminishes and approaches zero at ε_F. This approximation for Σ contains as a parameter the product of the electron–excitation coupling strength and the average amplitude of the excitation spectrum. It has been fitted to reproduce the measured width of the peak in the $\alpha = 7^\circ$ curve.

Figure 7 exhibits our theoretical results. For angles α above 5° we find remarkable agreement with experiment. The deviations for the 4° and the 5° curves whose peak features are caused by band 36 show, on the other hand, that our LDA–SIC band structure does not describe all of the details of the near-ε_F region correctly. It is worthwhile to discuss the contributions of the bands in some detail. In the $\boldsymbol{q}$-region probed by the 4° curve, band 36 crosses the FS, the main peak at 0.38 eV below ε_F is related to band 35, and band 34 gives rise to the shoulder on the left-hand side of this peak. At $\alpha = 6^\circ$, band 35 has moved to -0.17 eV, band 34 does not give rise to a distinct peak, and band 36 contributes negligibly. The $\alpha = 7^\circ$ curve hits a $\boldsymbol{q}$-region where band 35 crosses ε_F. The sharp structure is predominantly caused by band 35, whereas the amplitude of band 34 is rather small. Band 33 is responsible for the rising magnitude of the cross section towards increasing binding energies. Though band 35 lies above the Fermi level for $\alpha = 8^\circ$, its contribution is close to that provided by band 34. The peak in the 9° curve, on the other hand, is entirely due to band 34, whereas band 33 is still 0.7 below ε_F. We conclude that matrix element effects and band broadening should be taken into consideration when trying to trace bands on inspecting experimental curves.

4. Calculations for Sr_2RuO_4

4.1. The LDA band structure

We performed band-structure calculations, applying the scalar relativistic LMTO–ASA method to this case of a bct lattice and using the lattice parameters measured by Vogt and Buttrey (1995). The Sr 4p and the O 2s semi-core states have been put into the first panel, whereas the angular momenta of the basis set in the second panel went up to $l_{max} = 3$ for the Ru and the Sr atoms, and to $l_{max} = 2$ for the oxygens. The resulting total DOS together with the partial DOS of the different types of atom are shown in figure 8. The states in the pronounced structure between 8.8 and 2 eV below ε_F are of mainly of oxygen p character with relatively small admixtures of Ru d and Sr s contributions. The planar oxygens dominate between -8.8 eV and -4 eV, while the apex oxygens cause the high-peak structure between -4 eV and -2 eV. The pronounced double-peak feature in the vicinity of ε_F is due to Ru d contributions with non-negligible amplitudes of O-apex p and O-in-plane p characters in the lower and higher features, respectively. Sr s, p and d contributions start to dominate at 4 eV above the Fermi level. Since the Fermi level falls at the position of a steep rise of the DOS curve, $n(\varepsilon_F)$ depends sensitively on the details of the calculation. We obtain the value 75.05 (Ru: 55.02, O in plane: 15.08, O apex: 2.71, Sr: 2.19) states Ryd^{-1}/unit cell. The most significant sheets of the FS are due to bands 13, 14 and 15, while band 16 whose bottom falls 0.4 eV below ε_F is of minor importance. In figure 9 we show these bands along the Γ–M–Z–X–Γ path.

Our results are in general agreement with those obtained by Oguchi (1995), who

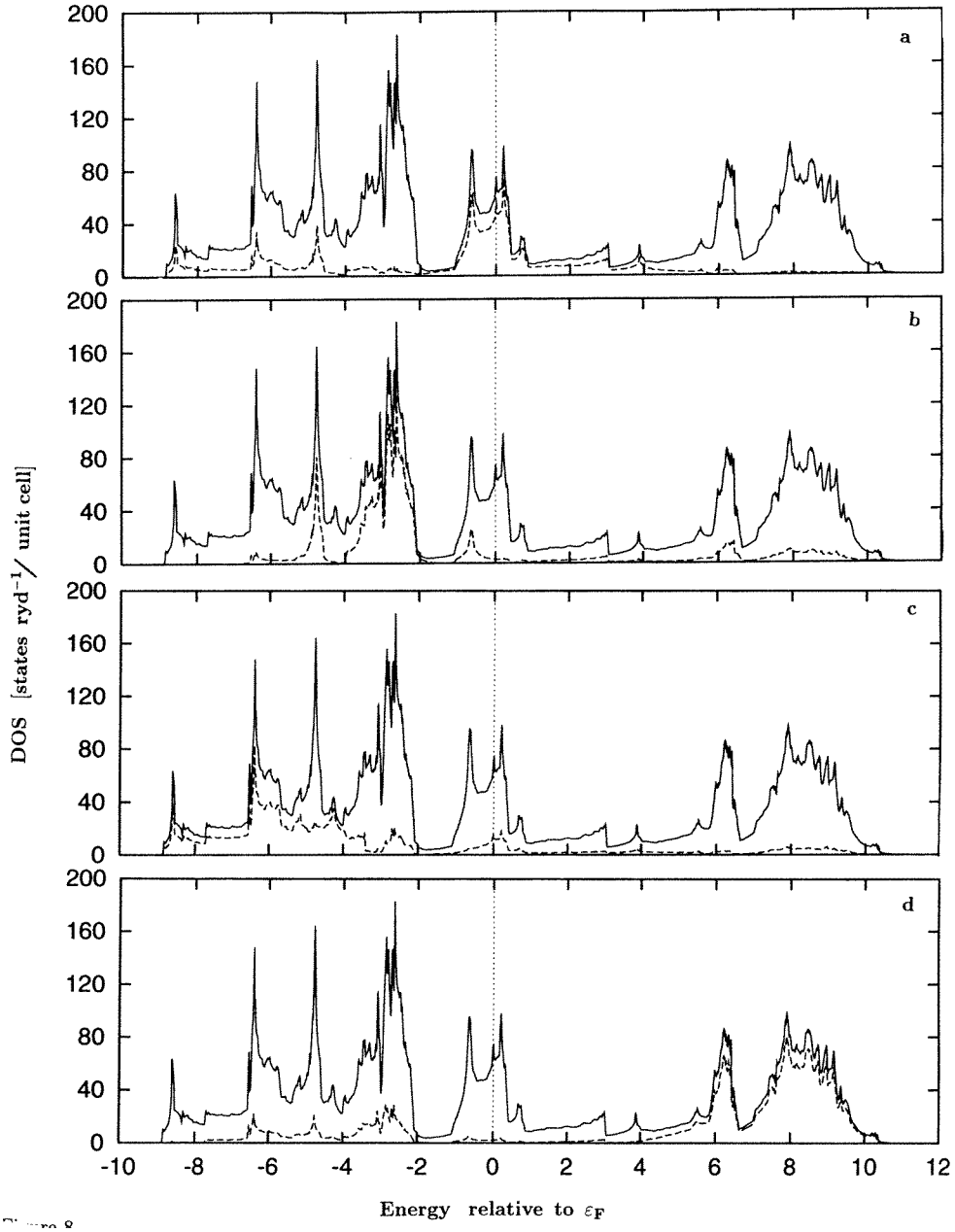

Figure 8. The LDA band structure of Sr_2RuO_4: densities of states. Solid lines: total DOS. Broken lines: partial DOS. (a) Ru; (b) apex O; (c) planar O; (d) Sr.

calculated the LDA band structure of Sr_2RuO_4 using the LAPW method. His Fermi level hits the same DOS feature as ours, but he gets a somewhat lower value for the DOS at ε_F ($n(\varepsilon_F) = 59.3$ states Ryd^{-1}/unit cell). Also the shapes of his bands 13 to 16 are similar, except that the bottom of band 16 is slightly above ε_F. The DOS curves resulting from the LAPW calculation of Singh (1995) fit into this picture. At some energies they exhibit

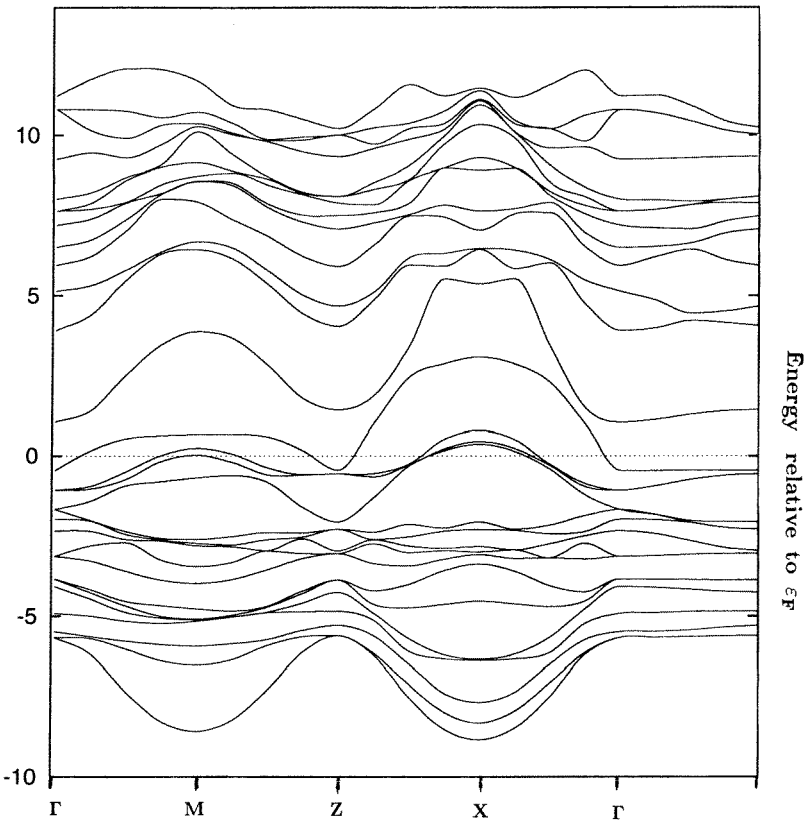

Figure 9. Sr_2RuO_4: bands 1–29 along the path Γ–M–Z–X–Γ–Z.

rather pronounced spiky features, and in contrast to our findings his Fermi level lies at the lower peak of the Ru d-dominated structure near ε_F.

4.2. ARPES cross sections

Our calculations aim at interpreting measurements of Cummins *et al* (1996). They used single crystals split such that the topmost surface layer consists of apex oxygen atoms and Sr atoms positioned slightly (0.382 au) below. In contrast to the case for $YBa_2Cu_3O_7$, the two surfaces resulting from the cleave are equivalent. The resolutions of their equipment amounted to 200 meV in energy and to 1° in angle, their photon energies varied between 25 eV and 70 eV, and $\boldsymbol{e}_r$ was parallel to the surface normal. Their curves are displayed in figure 10(b) and exhibit essentially three more or less pronounced features immediately below, at about 3 eV, and at 6 eV below ε_F. Especially striking is the resonance-like dependence of the amplitude of the intermediate peak at a photon frequency near $\omega = 40$ eV. The results of our calculations are shown in figure 10(a). As in the case of $YBa_2Cu_3O_7$, we introduced an average band broadening, the best fit to the widths of the experimental curves yielding the value $\Gamma_\Sigma = 0.3$ eV. The main features of the measurements are clearly reproduced by the theoretical curves. We find three structures at nearly the experimental positions. The amplitudes of the low-energy peaks diminish on increasing the photon

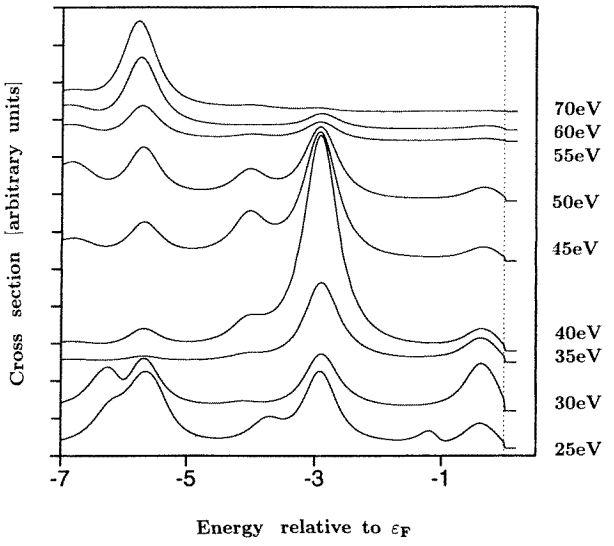

(a)

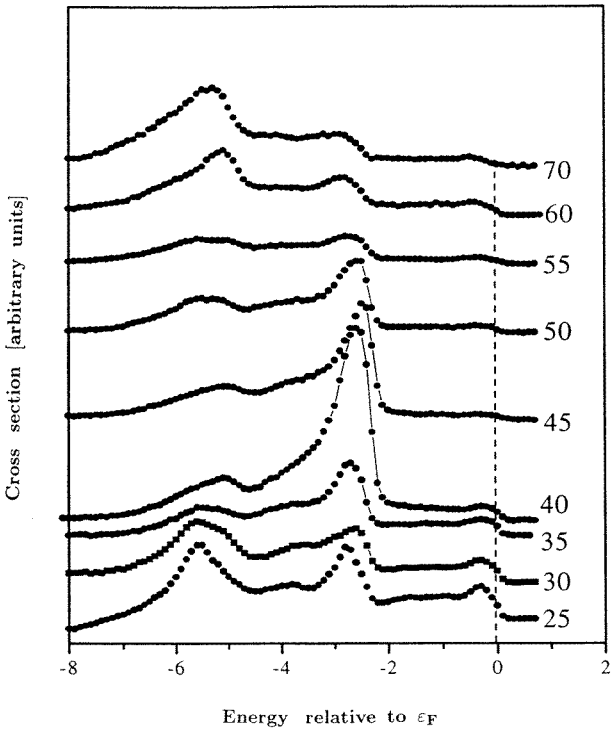

(b)

Figure 10. (a) Cross sections of Sr_2RuO_4 for photon frequencies between 25 eV and 70 eV evaluated including band broadening. (b) Experimental cross sections of Sr_2RuO_4 for photon frequencies between 25 eV and 70 eV (measurements of Cummins *et al* 1996).

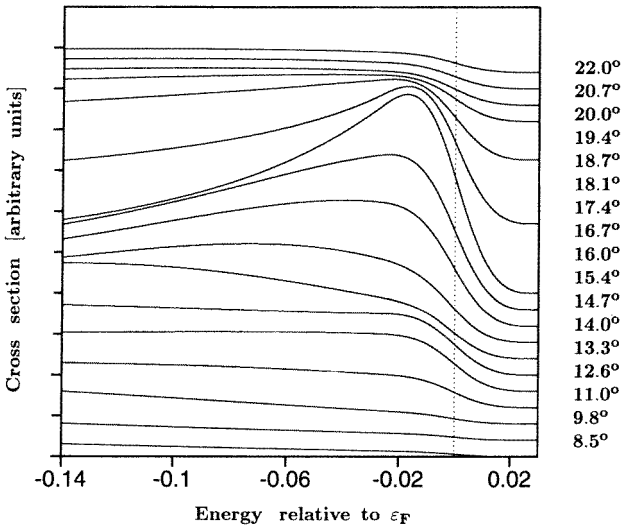

(a)

Figure 11. Calculated cross sections of Sr_2RuO_4 in the vicinity of the Fermi level for $\boldsymbol{k}_\parallel$ in the (1, 1) direction. (a) Total cross section. (b) The contribution of band 13. (c) The contribution of band 14. (d) The contribution of band 15.

energies from 25 eV to 40 eV and start to recover for higher ω-values. Also, the decrease of the amplitude of the near-FS structure beyond $\omega = 35$ eV is in accordance with the measurements. Especially gratifying, however, is the ability of the theory to explain the dramatic increase of the amplitude of the intermediate peak around $\omega = 40$ eV as a strongly photon frequency-dependent interference effect between the partial waves emerging from the individual atoms and modulating the matrix elements of our lowest-order cross section formula. Yokoya *et al* (1996) performed experiments for photon energies between 21 eV and 60 eV under the same conditions as were used by Cummins *et al*, and obtained practically the same results (figure 2 of their paper). They interpret this effect as the manifestation of resonant photoemission, involving the Ru 4p semi-core state and a correlation satellite of the Ru 4d band. This is in contrast to our explanation resulting from a theory that has not incorporated such higher-order processes. Yokoya *et al* exclude any alternative explanation of this phenomenon by using the following argument: the variation of the z-component, q_z, of the $\boldsymbol{q}$-vector (equation (7)) for the range of photon energies covered by their experiment amounts to three times the extent of the Brillouin zone in the z-direction. Any variation in the measured intensity due to band dispersion in this direction should therefore show up three times in their results. The strong dependence of our matrix elements on photon energy, on the other hand, leading to the marked enhancement of our calculated cross section at around $\omega = 40$ eV at a binding energy near 3 eV, has nothing to do with band dispersion. It is rather caused by the dependence of the value of the $\boldsymbol{k}$-vector entering the matrix element, $M_\lambda(\boldsymbol{q}, \boldsymbol{k})$, (equation (8)) on ω for a fixed binding energy. This dependence leads to a constructive interference of the individual atomic contributions to M_λ (equation (8)) for $\omega = 40$ eV, but a destructive interference for both $\omega = 35$ eV and $\omega = 45$ eV.

To address the measurements of Lu *et al* (1996), investigating the neighbourhood of ε_F, we again introduce band-dependent self-energies whose imaginary parts are proportional to the band-related partial DOS some 10 meV apart from the Fermi level. As in the

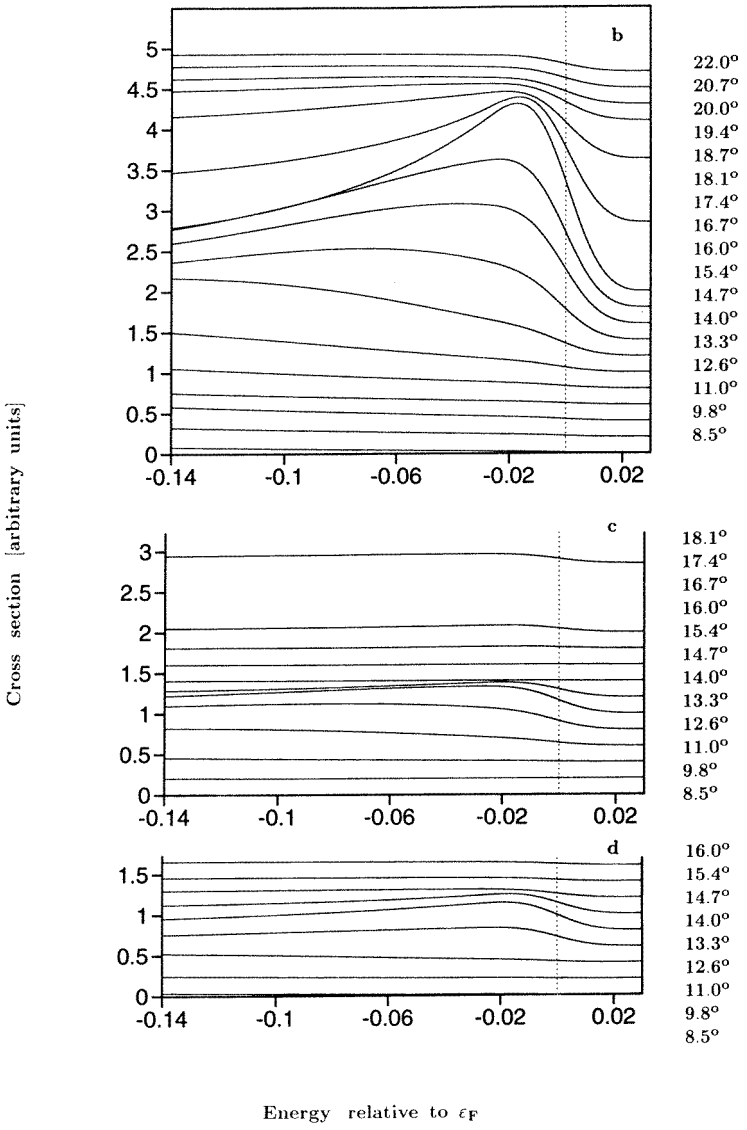

Figure 11. (Continued)

case of $YBa_2Cu_3O_7$, one parameter remains to be fitted to the width of some feature in the measured curves. The parameters of this experiment (figure 1(a) of their paper) are: resolutions: 22 meV in energy, 1° in angle; $\omega = 16.85$ eV (unpolarized photons); $\boldsymbol{k}_{\parallel} = (1, 1)0.514\sqrt{E}\sin\alpha$ (Å) with α varying between 8.5° and 22.0°. Thus the near-FS region in the Γ–X direction for binding energies up to 150 meV is probed by this measurement. Our results for the total cross section are displayed in figure 11(a), whereas figures 11(b), 11(c) and 11(d) show the individual contributions of bands 13, 14 and 15, respectively. They describe the important features of the experiment correctly. For small angles α the theoretical curves are rather structureless. With increasing angle the step near ε_F grows. The 15.4° curve starts to develop a broad peak at binding energies near 140 meV,

which sharpens and moves towards the FS when increasing α. At $\alpha = 18.1^\circ$ it crosses the Fermi level. For larger angles the curves rapidly flatten out. The broad humps in the 20.7° and in the 22.0° curve are due to lower energy bands not crossing the FS. It is worthwhile to consider the behaviour of individual bands in more detail. Apart from a tiny amount due to band 12, bands 13 to 15 provide the main contributions, but their amplitudes are very different and sensitively energy dependent. Band 15 dominates in the curves for angles between 12.6° and 14.0°. It crosses the Fermi level near the 14.0° curve and its contribution is negligible beyond $\alpha = 15.4^\circ$. Band 14 behaves rather strangely: its amplitudes in the 12.6° to 14° curves are significant, and on moving towards the FS they sharpen. However, beyond $\alpha = 14.7^\circ$, before the region between 15.4° and 16.0°, this band reaches ε_F, and its contribution decreases dramatically. In contrast to band 14, band 13 shows a regular behaviour: on moving towards ε_F its amplitude sharpens and increases, approaching its maximum at 17.4°, shortly before it reaches the FS near 18.1°; and it becomes negligible beyond 20.7°. These findings tell us that it is sometimes hard to follow all of the bands on inspecting experimental curves, since contributions may be depressed by matrix element effects, as is the case with band 14 in our example. It is therefore helpful to pursue both the changes, σ_m, in the heights of the near-FS peaks and the magnitudes, σ_F, of the measured cross sections at ε_F as functions of α. Our calculations and additional model investigations show that for a curve indicating band crossing, the ratio σ_m/σ_F reaches a maximum, and this criterion is also valid for bands providing low amplitudes. Applying this additional information to the experiment of Lu *et al*, we conclude that they observe the following three band crossings: of band 15 slightly above 14°, of band 14 between 15.4° and 16.0°, and of band 13 very near to 18.1°. As additional calculations show, the amplitude of band 14 quickly recovers with increasing deviation of $\boldsymbol{k}_\parallel$ from the (1, 1) direction, making it more easily detectable. This again is in nice agreement with experiment.

5. Summary

In this paper we described a simplified formalism for calculating angle-resolved photoemission cross sections. If it works, a rather direct relationship between measured curves and bulk electronic structures expressed by the one-particle Green function can be established. As our applications to the compounds $YBa_2Cu_3O_7$ and Sr_2RuO_4—materials of considerable interest in connection with high-temperature superconductivity—show, we are able to explain interesting features of the experiments.

When, e.g., comparing our calculations for $YBa_2Cu_3O_7$ to the measurements of Sakisaka *et al*, we made the unexpected observation that LDA, known to describe FS properties well, does not seem to work as satisfactorily at larger binding energies. Since the results obtained using the LDA–SIC band structure, on the other hand, show reasonable agreement, we assume that adding SIC is a sensible extension of the LDA to account for Coulomb correlation effects in this kind of system. We also demonstrated that cross sections related to inequivalent crystal surfaces resulting from cleaving in the process of sample preparation may differ significantly. When comparing measurements of groups mentioned in the present paper, this aspect should be taken into account.

Despite the fact that our theory considers only bulk states, we observe pronounced peaks at approximately 1 eV below the Fermi level for $\boldsymbol{q}$ near the Γ, the X and the Y points, belonging to different bands. Furthermore, the shapes of our theoretical curves fit reasonably well to the experiments of Tobin *et al*. Manzke *et al* (1991) on the other hand, who likewise observed these peaks in the vicinity of 0.92 eV below ε_F, interpret them as originating from surface states. Our calculations show the possibility of an alternative

explanation.

We also investigated the behaviour of the matrix elements in detail: depending on the characters of the electronic states and on phase factors, they weight the bands very differently and may strongly enhance some groups of bands and nearly extinguish others. Sometimes these features vary rapidly with photon energy, observation direction and binding energy. On in this point also, our calculations agree with experiment, especially in cases where these effects are dramatically pronounced.

Finally, we studied the influence of self-energy corrections such as band broadening on the shape of the cross sections; these turned out to be of greater importance than finite experimental resolutions. These kinds of investigation yielded rough estimates of the magnitude of average as well as of band-specific broadening in the substances considered, and may be of help in testing results of microscopic theories on the coupling between electrons and relevant excitations.

Our results for Sr_2RuO_4, gained exclusively on the basis of the LDA band structure, suggest that correlation effects in this substance are less important than in $YBa_2Cu_3O_4$.

In conclusion, we hope to have shown that there exists an intimate connection between bulk Green functions and ARPES cross sections and that it is worthwhile to try to interpret experiments on the basis of the simple theory presented in this paper as a first step before invoking programs treating the surface more realistically.

References

Cummins T R, Schmidt M, Gopinath C S, Lu D H and Schuppler S 1996 unpublished

Feibelman P J and Eastman D E 1974 *Phys. Rev.* B **10** 4932

Harm S, Mante G, Manzke R, Fink J and Skibowski M 1992 *Acta Phys. Pol.* A **82** 349

Keldysh L V 1965 *Sov. Phys.–JETP* **20** 1018

Ley L and Cardona M 1979 *Photoemission in Solids* (Heidelberg: Springer)

Lindroos M and Bansil A 1991 *J. Phys. Chem. Solids* **52** 1447

Liu R, Veal B, Paulikas A, Downey J, Shi H, Olson C, Gu C, Arko A and Joyse J 1992 *Phys. Rev.* B **45** 5614

Lu D H, Schmidt M, Cummins T R, Schuppler S, Lichtenberg F and Bednorz J 1996 *Phys. Rev. Lett.* **76** 4845

Manzke R, Mante G, Claessen R and Skibowski M 1992 *Surf. Sci.* **269+270** 1066

Manzke R, Mante G, Claessen R, Skibowski M and Fink J 1991 *Physica* C **185–189** 843

Oguchi T 1995 *Phys. Rev.* B **51** 1385

Pendry J B 1976 *Surf. Sci.* **57** 679

Pickett W E 1989 *Rev. Mod. Phys.* **61** 433

Pickett W E, Cohen R E and Krakauer H 1990 *Phys. Rev.* B **42** 8764

Sakisaka Y, Komeda T, Maruyama T and Onchi M 1989 *Phys. Rev.* B **39**4 2304

Schroeder N, Weiss S, Boettner R, Marquardt S, Ratz S, Dietz E, Gerhardt U, Ecke G, Roessler H and Wolf Th 1993 *Physica* C **218** 220

Shen Z X and Dessau D S 1995 *Phys. Rep.* **253** 1

Singh D J 1995 *Phys. Rev.* B **52** 1358

Svane A 1992 *Phys. Rev. Lett.* **68** 1900

Svane A and Gunnarsson O 1990 *Phys. Rev. Lett.* **65** 1148

Szotek Z, Temmerman W M and Winter H 1993 *Phys. Rev.* B **47** 4029

——1994 *Phys. Rev. Lett.* **72** 1244

Temmerman W M, Szotek Z and Winter H 1993 *Phys. Rev.* B **47** 1184

Tobin J, Olson C, Gu C, Liu J, Solal F, Fluss M, Howell R, O'Brien J, Radousky H and Sterne P 1992 *Phys. Rev.* B **45** 5563

Veal B W and Gu Chun 1994 *J. Electron Spectrosc. Relat. Phenom.* **66** 321

Vogt T and Buttrey D 1995 *Phys. Rev* B **52** 14 52

Yokoya T, Chainani A, Takahashi T and Katayama-Yoshida H 1996 *Phys. Rev.* B **53** 8151